The use of 1D carbon nanotube interacting with caffeine molecules for applications in solar cells: Structure optimisation, Raman analysis and optoelectronic properties

Anass El Fatimy, Mourad Boutahir, Abdellah El Attar, Konstantinos Termentzidis, Abdelhai Rahmani, Abdelali Rahmani

The use of 1D carbon nanotube interacting with caffeine molecules for applications in solar cells: Structure optimisation, Raman analysis and optoelectronic properties.

Anass El fatimy[1,2*], Mourad Boutahir[1,3], Abdellah El Attar[3], Konstantinos Termentzidis[2], Abdelhai Rahmani[1], Abdelali Rahmani[1]

[1]Advanced Material and Applications Laboratory (LEM2A), Moulay Ismail University FSM-ESTM-ENS, BP 11201, Zitoune, Meknes, 50000, Morocco.

[2]Laboratoire CETHIL UMR 5008, CNRS, INSA of Lyon, Un. Claude-Bernard Lyon 1, NSA de LYON 9 Rue de la Physique, LYON, 69100, FRANCE.

[3]Ecole Normale Supérieure, Université Moulay Ismail, BP 3004, Toulal, Meknes, 50000, Morocco.

Abstract

This study proposes a promising candidate for organic solar cells through the creation of a novel nano-hybrid system composed of caffeine molecules encapsulated within a semiconducting single-walled carbon nanotube known as NT14 (14,0). The stability and optoelectronic properties of this hybrid system, designated as CA@NT14, were thoroughly investigated. We determined the optimal diameter for the NT14 nanotube using molecular mechanics, Density Functional Theory, spectral moment's method, and bond polarizability model, finding it to be approximately 1.18 nm. The encapsulation's impact on the Raman-active modes, specifically the radial breathing mode and tangential mode, was analyzed through Raman spectra calculations, revealing structural stability and charge transfer from CA to NT14. Notably, the NT14's Fermi level position increased upon encapsulation, indicating charge transfer and a type-II band alignment. The study further examined the bandgap characteristics of the hybrid system, finding that the encapsulation of CA within semiconducting NT14 nanotubes minimally impacts the nanotube's bandgap, thus retaining its excellent visible

light absorption properties. Conversely, encapsulating CA within metallic nanotubes significantly reduces their bandgap, limiting their light absorption range. The nonresonant Raman responses of NT14 pre- and post-encapsulation corroborated the charge transfer between CA and NT14. Future research will focus on computing the electronic transport characteristics, transmission spectra, I-V characteristics, and yield of CA@NT14 using DFT and Non-Equilibrium Green's Function (formalism. An experimental study will be conducted to validate these theoretical findings. These results indicate the potential of CA@NT14 hybrids as effective active layers in organic solar cells, highlighting their significance in advancing optoelectronic applications.

Keywords: SWNT, Caffein, organic solar

1 Introduction

Perovskite solar cells are very promising photovoltaic sector [1, 2]. But they suffer from a major handicap "like Organic solar cells (OSCs)", of rapidly degrading under the effect of humidity,poor charge transport [3–6] heat, ultraviolet and long term stability [7–9]. An effect counteracted by the addition of caffeine during manufacture, the researchers from the University of California have just discovered by chance [10]. A few drops of coffee in your solar cell? It's the brainchild of Rui Wang and his colleagues at the University of California (UCLA) to improve the efficiency and durability of hybrid organic/inorganic perovskite solar cells, where it all started with a machine joke. coffee by asking the question: if caffeine boosts our energy, why couldn't it do the same for perovskite?[10] Indeed, during the manufacture of the cell, the addition of caffeine molecules made it possible to eliminate structural defects of the crystal and to facilitate the transfer of charge inside the cell, increasing its yield from 17% at 20.25% [11–14]. Above all, the cell proves to be stable over time, which prevents degradation at high temperature. Whereas in normal times, the cells lose 60 % of their efficiency after 175 hours at a temperature of 85°C, those enriched with caffeine prove to be thermally stable for more than 1300 hours of exposure. The cells doped with caffeine thus have an extended lifespan and a higher efficiency. While caffeine seems to significantly improve the performance of cells that use perovskite to absorb sunlight[10], will it be useful for other types of solar cells, especially those that are the subject of this manuscript where the SWNTs Will be used to absorb light. Can the encapsulation of caffeine molecules in SWNTs make it possible to develop a system that takes advantage of both the physical properties of SWNTs and those of caffeine molecules, in the sense that the stability presented by caffeine, combined with the wall-protective advantage of carbon nanotubes seems to play a crucial role in the development of photovoltaic technologies in terms of high efficiency and long-term stability[15–20]. In this context, we are thinking about the encapsulation of this type of molecule inside the SWNTs as well as the hybrid nT@SWNTS (n=2,4,6). For the empty SWNT(11.0)(NT11) shows a band gap E_g around 1.03 ev and E_g of 0.78 after encapsulation of two molecules of thiophene [21–24].The nT@NT11 exhibits a drop in

E_g , which gets more pronounced as the molecular chain lenght increases ,they also calculated the absorption coefficient of thiophene molecules encased in carbon nanotubes and discovred that NT11 has a significant absorption behavior in these hybrids not just in the UV-visible region ,but also in the near-infrared spectrum. In comparaison with other structures, these hybrids featured notable properties [21, 25, 26]. They also anticipated a photovoltaic performance after calculating the power conversion The effectiveness of these hybrid systems was examined, and it was found that the yield improved by approximately 4.98%. Initially, when two thiophene molecules were enclosed within carbon nanotubes, the yield was 1.3%. However, when six thiophene molecules were introduced into single-walled carbon nanotubes, the yield increased to 6.8% [21]. This study focuses on the encapsulation of a chemical compound known as caffeine (CA), specifically 1,3,7-trimethylxanthine. In this study, we successfully encapsulated caffeine within the hollow space of SWNTs, resulting in CA@SWNT. This novel hybrid system shows great potential as a photoactive material in organic solar cells (OSCs). By employing this technique, we can effectively combine the desirable physical properties of both systems without causing any mechanical or chemical harm. It is anticipated that this approach will contribute to achieving high efficiency and stability in OSCs in the future, from this perspective [27, 28]. In a recent study conducted by Rui Wang and his team, they incorporated caffeine, which is the active component found in coffee, into the active materials of inorganic perovskite solar cells to enhance their performance and thermal stability. The inclusion of caffeine resulted in a significant improvement in thermal stability, increasing the duration from 300 hours without caffeine to 1300 hours with caffeine at a temperature of 85°C under a nitrogen atmosphere. Additionally, the solar cells achieved a champion stabilized efficiency of approximately 19.8%. As a result of these advancements, a remarkable power conversion efficiency (PCE) of up to 25.25% was accomplished [10]. We focused on one chaine caffeine molecules encapsulated in a single wall carbone nanotube (14,0) (NT14) to exploit these filled nanohybrid systems' beneficial qualities as active layer materials for OSCs.

The paper is organized as follows: In Section 2, a computational approach employed in the study is described. Section 3 is divided into two parts. The first part focuses on the computation of optoelectronic properties of individual caffeine (CA) molecules. The second part investigates the Raman spectra calculations for both isolated caffeine molecules and caffeine encapsulated within carbon nanotubes (CA@NT14), along with the empty NT14. Additionally, the article provides calculations of the optoelectronic characteristics of the pristine NT14, CA@NT14, and CA2@NT14 nano-hybrid systems. Finally, the paper concludes by presenting a summary of the key research findings.

2 Methods and model

The polarizability tensor and the dynamic matrix (DM) of a molecular system allow respectively the determination of the intensities and the frequency positions of the characteristics Raman, and the knowledge of these two quantities is essential for the theoretical evaluation Raman spectra. However, the calculation of these two quantities

cannot be done using ab initio methods, because the large number of atoms which then requires a huge calculation time.
The process begins with calculating the dynamic matrix of the CA molecule using Density Functional Theory (DFT). In a subsequent step, the dynamic matrix of the NT14 is determined using the force constant model known as the 4-neighbor model (4NNFC), as introduced by Saito et al. [29–33]. The third step involves computing the matrix dynamics of the coupling by employing the Lennard-Jones potential. This potential enables an accurate description of Van der Waals interactions, as depicted in Figure 1. Thus, to build the dynamic matrix of CA@SNT14 hybrids, the adopted solution was to go through molecular dynamics, where the main difficulty is to have a field of force correctly set. However, the non-existence of such a force field which processes the hybrid system as a whole, forced us to adopt a three-step methodology drawing based on Density functional theory (DFT) and molecular dynamics, DFT and the local density approximation, as implemented in the SIESTA package, are used to compute the DM of the CA molecules [34–39]. A real space integration grid that corresponds to a 360 Ry plane wave cutoff was employed in conjunction with a double-singly polarized basis set with an energy shift of 50 meV for this purpose. The force constant model developed by Dresselhaus et al[29] package [34, 40] is used to calculate the dynamic matrix of NT14.

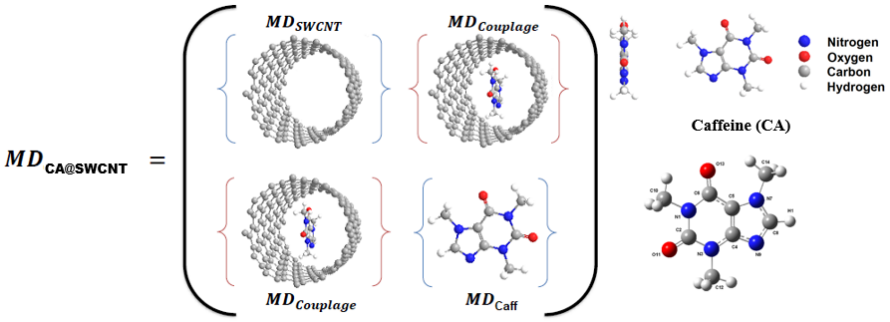

Fig. 1: Construction of the total dynamic matrix of the hybrid system from the dynamic matrices of these subsystems

In this study, our objective was to determine the optimal diameter of nanotubes for encapsulating caffeine (CA) molecules. The primary mode of interaction between the encapsulated molecules and nanotubes is through van der Waals (vdW) interactions. The Lennard-Jones potential(LJ), as described by Rahmani et al. [41], serves as the most suitable model to characterize these interactions. Hence, we conducted energy minimization calculations on hybrid single-walled carbon nanotubes (SWNTs) considering various diameters and chiralities, utilizing the Lennard-Jones potential. The structure of the carbon nanotube is obtained by the self-winding of graphene, forming a hollow cylinder characterized by a pair of integers (n, m) that determine its structural properties. On the other hand, the geometry optimization of the CA molecule

was performed using the SIESTA method with the LDA exchange-correlation functional. In our calculations, we considered two models of CA molecules and CA@NT14 hybrids, as illustrated in Figure 3. First, we presented the geometry of an isolated CA molecule in two positions: a top view and a side view, as shown in Figure 3-a. Following this, we presented two distinct configurations of the hybrid system Figure 3-b. In the CA@NT14 hybrid, the CA molecule is placed vertically relative to the nanotube's axis. In the CA2@NT14 hybrid, the CA molecule is positioned horizontally relative to the axis of the nanotube.

To optimize the structural geometry of the encapsulated systems, particularly the diameter of the SWNT for different angles of the CA molecule inside the tube, we employed a practical representation of the intermolecular van der Waals (vdW) interactions known as the Lennard-Jones (LJ) potential. After conducting calculations at different angles of the CA molecule inside the SWNT, it was observed that the results remained consistent. Therefore, two distinct configurations, namely the vertical and horizontal orientations, were selected to assess the physical properties of the hybrid systems. The findings indicate that the CA molecule confined within the NT14 nanotube exhibits an optimal diameter of approximately 1.18 nm. This diameter corresponds to the most stable structure of the encapsulated system (see Figure 2).

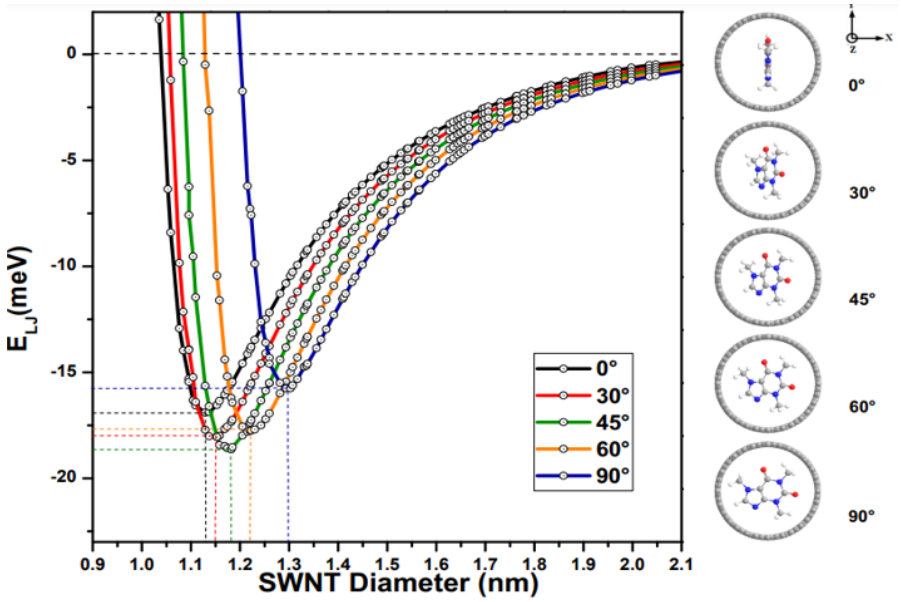

Fig. 2: Lennard Jones potential as a function of the tube diameter for CA@SWNT hybrid systems, and an illustration of the Caffeine (CA) encapsulation in different angle inside SWNTs.

$$U_{LJ} = 4\varepsilon_{ij}\left[\left(\frac{\sigma_{ij}}{r_{ij}}\right)^{12} - \left(\frac{\sigma_{ij}}{r_{ij}}\right)^{6}\right] \quad avec \quad \varepsilon_{ij} = \sqrt{\varepsilon_i \varepsilon_j} \;\; et \;\; \sigma_{ij} = \frac{1}{2}(\sigma_i + \sigma_j) \qquad (1)$$

The indices i and j represent the two atoms between which the interaction is calculated while the parameters, ε and σ, respectively represent the depth of the potential well and the van der Waals radius . These parameters are given in Table 1

Table 1: Lennard-Jones parameters for hydrogen, carbon, nitrogen and oxygen atom

Atom	ε_i (meV)	σ_i (nm)
H	0.86	0.178
C	5.16	0.33
N	6.88	0.312
O	8.6	0.285

Then, we must determine the derivatives of the polarizability tensor (responsible for the intensity Raman lines) with respect to atomic displacements. We have therefore used the model of bond polarizability to calculate the line intensity of Raman scattering spectra in a non-resonant process ,i.e. assuming that the excitation energy is very small with respect to the energies of the electronic transitions of the material studied. This model was successfully applied for the calculation of the intensity of non-resonant Raman scattering spectra of a wide variety of systems [41–43].

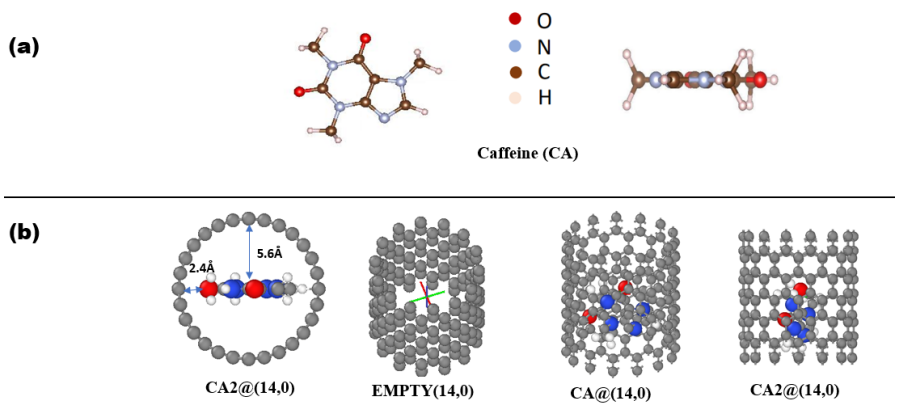

Fig. 3: Schematic representation of the encapsulation of caffeine (CA) molecules inside NT14 ,the empty NT14 and characteristic distances after minimization of energy:(a) CA. (b) CA@NT14 , CA2@NT14 and NT14. The highlighted distances values are provided in nanometer (nm)

3 Results and discussion

3.1 Structural and physical properties of isolated CA

3.1.1 Structural properties

We analyze the stability and structural features of the pure CA molecule, and we anticipate the most stable forms for this molecule. Finally, we report on the polarization calculation, which is defined as the contribution of the closest linkages. The values of the polarizability parameters of bonds used in this study for the CA molecule (see figure1 for labels atoms) are given in Table 2. The frequencies of the active modes in Raman are deduced from the position of the peaks in the Raman spectra (the width of the lines Lorentzian of each peak is fixed at 1.7 cm^{-1}).

Table 2: Values of bond polarizability parameters for the CA molecule and the carbon nanotube

	$\bar{\alpha}$ ($\AA^2$)	$\bar{\beta}$ ($\AA^2$)	$\bar{\gamma}$ ($\AA^3$)
CA			
N1-C2	194,0	165	1.65
C2-N3	686.07	85.62	24.51
N3-C4	-175.06	107.75	5.72
C4-C5	194.04	282.34	0.95
C5-C6	1681.60	113.52	3.57
C6-N1	0	0	0
C5-N7	0	0	0
N7-C8	0	0	0
C8-N9	0	0	0
N1-C10	0	0	0
C2-O11	0	0	0
N3-C12	0	0	0
C6-O13	0	0	0
N7-C14	0	0	0
C8-H1	0	0	0

parameters: $\bar{\alpha} = 2\alpha_p^{'} + \alpha_l^{'}$,$\bar{\beta} = \alpha_l^{'} - \alpha_p^{'}$ and $\bar{\gamma} = \frac{(\alpha_l + \alpha_p)}{r}$ or any other form of bond.

3.1.2 Electronic and optical behavior of CAs

To ensure a reliable interpretation of our computed physical properties in the hybrid systems, it is crucial to have a comprehensive understanding of the characteristic behavior of caffeine molecules. With the objective of gaining insights, our calculations primarily focused on the electrical and optical aspects, including band structure, density of states, and optical absorption spectra. The goal was to explore the potential use

Table 3: HOMO (eV), LUMO (eV), Fermi energy (FE) (eV), and Bandgap energy (eV) of the pristine CA molecule.

	HOMO(eV)	LUMO(eV)	FE(eV)	E_G(eV)
B3LYPB	-5.15	-0.12	-5.10	5.03
HSE06	-4.97	-0.34	-4.97	4.63
GGA	-4.30	-0.80	-4.30	3.50

of caffeine in organic solar cells (OSCs) to enhance their performance and thermal stability. In Table 3, we present electronic parameters such as HOMO (highest occupied molecular orbital), LUMO (lowest unoccupied molecular orbital), FE, and HOMO-LUMO gaps obtained for the pristine caffeine molecule using various exchange(XC) functionals (GGA, B3LYP, and HSE06). Notably, the FE of the caffeine molecule experiences an upshift when transitioning between different XC functionals. Specifically, When transitioning from the GGA functional to the B3LYP functional, a noticeable downward shift in the position of the FE is observed. This shift corresponds to FE of 4.30 eV, 4.97 eV, and -5.10 eV for the GGA, HSE06, and B3LYP functionals, respectively. The downward shift of the FE in the caffeine (CA) molecule when utilizing the B3LYP functional, in comparison to other xc functionals, indicates stronger electron-electron interactions or increased electron correlation effects. These effects can significantly impact the electronic properties and behavior of the CA molecule within an organic solar cell (OSC). They have the potential to influence reactivity, charge transfer processes, and energy levels, ultimately affecting the overall performance and characteristics of the OSC.

The transition from the B3LYP functional to the GGA functional resulted in a reduction of the HOMO-LUMO gap (E_g) for the caffeine (CA) molecule. When using the B3LYP functional, the E_g was approximately 5.03 eV. However, when switching from the HSE06 functional to the GGA functional, a more significant decrease in the HOMO-LUMO gap was observed. This suggests that the GGA functional may not fully account for electron correlation effects or exchange interactions within the system. On the other hand, the HSE06 and B3LYP functionals, being hybrid functionals that combine exact exchange and density functionals, provide a more accurate description of electronic correlations and interactions.This is evident in Figure 4-(a), which displays the electron density of states predicted by each functional for the CA molecule.

4-(b) illustrates the electron density distributions of the caffeine molecule, focusing on the total density, the highest occupied molecular orbital (HOMO), and the lowest unoccupied molecular orbital (LUMO). The total density plot at the top shows where electrons are most likely to be found in the molecule, with a color gradient indicating areas of higher (red) and lower (blue) electron density. The HOMO image highlights the regions where the molecule's highest energy electrons are located, typically involving electron-rich areas such as lone pairs on nitrogen atoms or π bonds in aromatic rings. The LUMO image, on the other hand, reveals where the molecule can accept

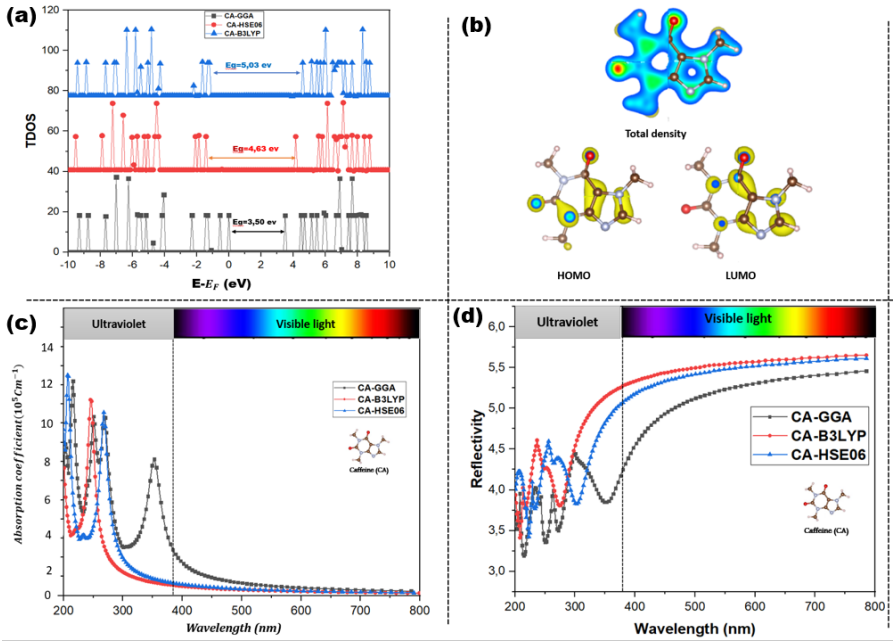

Fig. 4: Optolectronic properties of CA molecule: (a)Electronic density of states (DOS). (b) The obtained total density and HOMO-LUMO of CA .(c)Absorption spectra of CA molecule for all XC functionals (GGA,B3LYP,HSE06) . (d) reflectance spectrum of CA molecule for all XC functionals (GGA,B3LYP,HSE06)

electrons, often indicating potential sites for electrophilic attack, such as antibonding orbitals in π systems or on electronegative atoms like oxygen. Analyzing these plots provides insights into the chemical reactivity and stability of caffeine, with the energy gap between HOMO and LUMO (the HOMO-LUMO gap) being particularly crucial. A smaller gap suggests higher reactivity, as electrons can easily transition from HOMO to LUMO. Based on the findings by Laxman Pandey et al. [44], the increased orbital overlap between the highest occupied molecular orbital (HOMO) and lowest unoccupied molecular orbital (LUMO) in the caffeine (CA) molecule system contributes to an enhanced absorption coefficient. This effect is more clearly evident in the absorption spectra of the CA molecules. Figure 4-(c) displays the UV-visible absorption spectra of the caffeine molecule, which were calculated based on the electronic structure obtained using the GGA functional. When transitioning between different states of the xc functional, the bandgaps of the CA molecule decrease, leading to significant optical absorption in the UV light region. Compared to other xc functionals, the GGA functional results in a shift of the optical absorption towards longer wavelengths. This functional facilitates interband transitions, broadening the absorption range and increasing the relative absorption intensity of the CA molecule.
Despite significant absorption of both UV and visible light by the caffeine (CA) molecule, it is anticipated that not all energy will be fully absorbed, resulting in

some rays being reflected. Figure 4-(d) illustrates the overall reflectance of the CA molecule across different states of the xc functional. The molecule exhibits a narrowband reflectance within the range of 200-400 nm. In the UV region, there is a fluctuation in reflectance, with the GGA functional showing a minimum value of 3.1 percent. Overall, the reflectance spectra for the three states of the xc functionals exhibit similar behavior. The reflectance intensities of the B3LYP and HSE06 functionals are slightly higher than those of the GGA functional, as depicted in Figure 4-(d), indicating the stability of the CA molecule under UV radiation.

3.2 Stability of CA confined into NT14

3.2.1 Raman spectra of CA@NT14 hybrid system

To ensure a proper interpretation of the expected hybrid Raman spectra in the hybrid systems, a comprehensive and precise vibrational assignment of the experimental Raman fingerprints of caffeine (CA) molecules is necessary. This serves as a reference for comparison. Figure 5-(a) presents the predicted Raman spectra of the CA molecule up to 1760 cm^{-1}. However, there is no discussion regarding the frequency range (2900-3100 cm^{-1}) associated with the CH stretching vibration. Raman spectroscopy is a powerful technique for analyzing the structural, vibrational, and electrical properties of single-walled carbon nanotubes (SWNTs). SWNT Raman spectra exhibit two prominent characteristics. The first characteristic is referred to as the radial breathing mode (RBM), which involves the in-phase motion of carbon atoms in the radial direction. The RBM mode, positioned below 400 cm^{-1} (refer to Figure 5-(c)), can be utilized to determine the diameter distribution of nanotubes. The second characteristic is known as the G-band, located above 1500 cm^{-1}. Figure 5-(b) displays the computed ZZ-polarized Raman spectra of the CA@NT14 hybrid and empty NT14. Prior to comparison, the intensities of all spectra are adjusted for each NT14 and CA@NT14. Consequently, the Raman spectrum of the CA@NT14 hybrid initially appears to be a combination of the Raman spectra of the CA molecule and NT14. However, a more detailed analysis reveals that the low-frequency Raman lines in the CA@NT14 hybrid exhibit higher sensitivity to nanoconfinement. Specifically, the Raman spectrum of the hybrid CA@NT14 demonstrates a significantly weak intensity for the line at 67 cm^{-1}, which corresponds to the oscillating vibration of the CH3 groups in free CA molecule(s) (refer to Figure 5-(a)). This indicates that the interaction with the nanotube imposes constraints on the methyl groups. The location of the radial breathing mode (RBM) frequency in the filled nanotube (see Figure 5-(c)), which is at 178 cm^{-1}, remains the same as in the empty NT14. This RBM response is expected when the diameter of the nanotube provides suitable stabilization energy for the encapsulation of CA molecules.

Regarding to the empty NT14's high-frequency area where tangential modes (TM) are seen (figure5-(d)), The computed G-band is dominated by a single peak that has been identified as A1g (ZZ) TM and is located at 1589 cm^{-1}. The chirality dependency of this mode, where the G^+ peak is prominent for zigzag tubes and the G^- peak is dominant for armchair tubes, the appearance of two peaks (G^+ and G^-) when the chiral angle Θ increases from 0 (armchair tubes) to 30 (zigzag tubes) was already covered

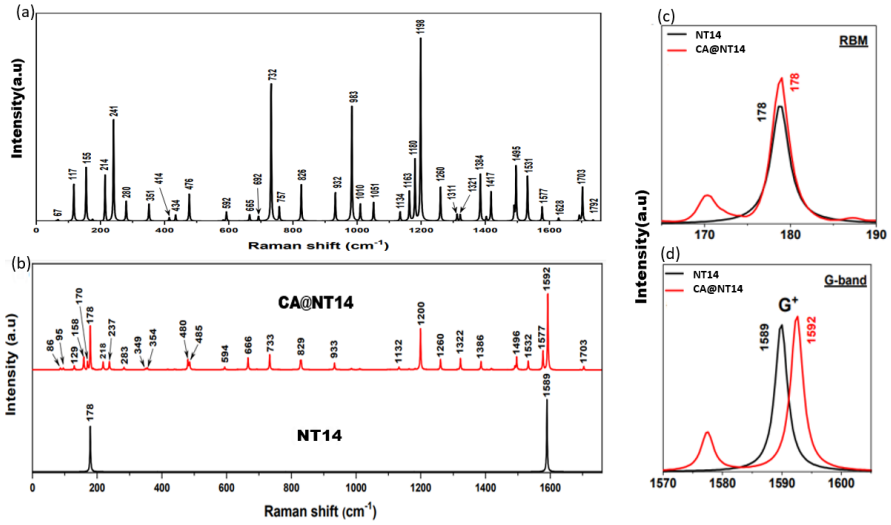

Fig. 5: Raman spectra calculations: (a)isolated CA molecule(s).(b) CA@NT14 haybrid system and pure NT14. (c) RBM range.(d) TM region

in detail in [45]. The peak location of the G-band is impacted by the encapsulation of CA molecule(s) (figure5-(d)). It demonstrates a considerable frequency upshift of the G^+ peak (LO mode) of 3 cm^{-1} with respect to the empty NT14. As a result, there is a charge transfer between the CA molecules and the nanotube's host. which the current estimate did not anticipate

The encapsulation of CA molecule(s) significantly affects the peak position of the G-band (see Figure 5-(d)). Specifically, there is a significant upshift of 3 cm^{-1} in the frequency of the G^+ peak (LO mode) compared to the empty NT14.

This unexpected shift in the G-band peak location indicates the occurrence of charge transfer between the CA molecules and the host nanotube, which was not initially anticipated in the current estimation

3.2.2 Optoelectronic properties of CA@NT14

The observed shift in the G-band mode provides evidence for the presence of charge transfer (CT) in the encapsulated devices of CA@NT14s. The encapsulation effect can lead to two primary types of alterations in the electronic properties of SWNTs: CT from molecules to SWNTs, resulting in a decrease in the SWNT FE, or CT from SWNTs to encapsulated compounds, leading to an increase in the SWNT's FE. The electronic properties, including LUMO, HOMO, gap, and FE, were calculated and reported for pure NT14, CA@NT14, and CA2@NT14 hybrids, as shown in Table 4. The FE of the empty NT14 and its shift after encapsulation are also presented. The data reveal that the FE of NT14 increases upon encapsulation with different configurations of the CA molecule, indicating a charge transfer (CT) from CA to NT14. The corresponding FE shifts are 0.06 eV and 0.11 eV for CA@NT14 and CA2@NT14, respectively. The HOMO-LUMO gaps (E_g) also demonstrate that

encapsulation reduces the difference between the HOMO and LUMO levels. The NT14 tube exhibits a E_g value of 0.73 eV. When the CA molecule inside the nanotube transitions from its front configuration to a horizontal shape, the E_g for the hybrid nano-systems significantly decreases compared to that of the NT14 alone. This can be clearly observed in the calculated electron densities of states of NT14 and the hybrid systems, as depicted in Figure 6-(a), with the FE set to zero.

Figure6-(a) illustrates how the total density of states (TDOS) of CA@NT14 and CA2@NT14 exhibit considerable differences from the original NT14 , which would causes NT14's conductance to very upon encapsulation . We discovered that bandgaps close to (E_f) get smaller and new local energy levels (molecular states of CA) arise,this implies that the encapsulation effect increased the conductivity of NT14. This progress is in line with the CT results which can be obviously seen from the electron density distributions of molecular orbitals wave-functions figure6-(b) shows a demonstration of the pure NT14 and the two hybrid systems in HOMO and LUMO.

Both the pure NT14 and the enclosed hybrid systems exhibit delocalized HOMO

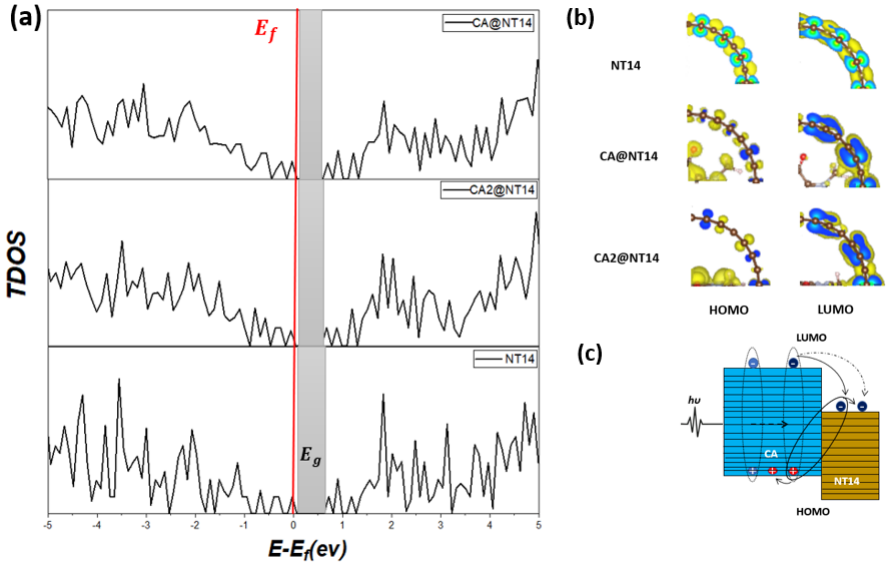

Fig. 6: Electronic behavior of the pristine NT14 tube and CA@NT14:a)Total electronic density of states.b)The calculated difference in electronic densities of the pure NT14, CA@NT14, and CA2@NT14 . c) schematic form of the Stepwise photoinduced electron transfer (PET) between CA and NT14 .

wave functions. Which CA molecules are the donor portion and the NT14 is the acceptor part, we notice that a extended delocalization of the HOMO was seen in the pure NT14 and when we switched from CA2@NT14 (the horizontal configuration of CA) to CA@NT14 (the front configuration of CA) hybrids. On the other side, their LUMO wave functions, are more concentrated at the pure NT14, suggesting that

Table 4: Energy gaps ,HOMO ,LUMO and FE of isolated NT14 ,CA@NT14 and CA2@NT14 hybrid nano-systems.

	HOMO	LUMO	FE	E_G
NT14	-3.4394	-2.7136	-3.3637	0.7259
CA@NT14	-3.3499	-2.6603	-3.2952	0.6896
CA2@NT14	-3.3042	-2.6196	-3.2506	0.6847

The Lennard-Jones potential(LJ), as described by Rahmani et al. [41], serves as the most suitable model to characterize these interactions. Hence, w

there occurred a CT from CA to NT14. As a result, the hybrid encapsulated systems contain type II heterojunctions (see figure6-(c);

The effective separation of the photogenerated charge carriers in bulk heterojunction OSCs is strongly impacted by such a type II band alignment. When exposed to light, the electrons from CA molecules may be directly excited to NT14, creating a functional charge separation between the two subsystems that is essential for boosting PCE of OSCs. Moreover, Laxman Pandet and al[44] found that the greater orbital overlap between HOMO and LUMO of CA@NT14 and CA2@NT14 hybrid systems contributes to the increased absorption effect. this effect could be clearly seen in the absorption curve of the hybrid systems. As shown in figure7-(a), the electronic structure derived with the GGA contaThank you very much for your recommendation. Please find the answers belowining vdWs interaction is used to determine the UV-visible absorption spectra of the empty NT14 and CA encapsulated systems. These hybrids exhibit considerable optical absorption not just in the UV-visible light area but also in the near-infrared spectral regions because to the NT14's short bandgap. Also, due to their smaller bandgaps than those of pristine NT14, the optical absorption curves of the hybrid systems shift toward the longer wavelength (figure7-(a)). More bound electrons participate in the interband transitions due to the configurations of CA contained in the NT14 bandgap.

We subsequently computed the dielectric functions of the pure NT14 tube and the CA encapsulated systems (CA@NT14 and CA2@NT14) (see figure7-(b)) using the electron energy levels and associated wave functions from the electronic structure simulations. As a function of photon energy, the imaginary and real components of the dielectric function were computed. The real part of the dielectric function suggests the electronic polarizability of the pure NT14 tube and the CA encapsulated systems which have the same characteristics in all energy regions with a maximum of peaks intensity of about 12 in the Infrared area. The fact that the pure NT14 and the CA encapsulated systems all show high peaks in the imaginary part of the dielectric function at photon energies of around 0.65 eV in the infrared region which suggests that the CA encapsulated systems can be employed as photonic sensors in this spectrum. Applications in electro-optical devices particularly in OSCs, are possible because to the semiconducting carbon nanotube's peculiar optical characteristics when filled with CA molecules (Table4).

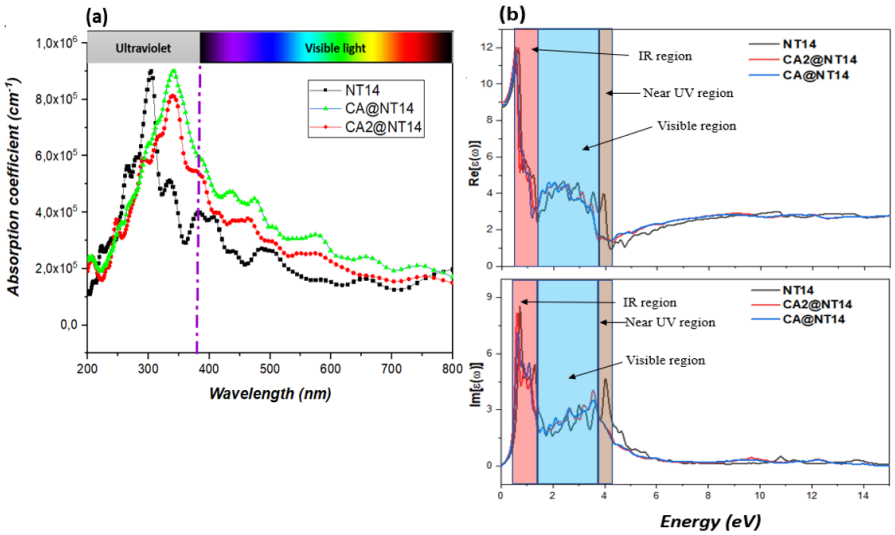

Fig. 7: (a)Absorption coefficient of the pure NT14 tube, CA@NT14 and CA2@NT14 hybrid nano-systems,(b)imaginary and real dielectric functions for the pure NT14 tube, CA@NT14 and CA2@NT14 hybrid systems

4 Conclusion

Semiconducting single-walled carbon nanotubes incorporating photoactive molecules are highly desirable due to their exceptional optoelectronic properties, particularly for applications in organic solar cells. In this study, we employed three computational methods to investigate the encapsulation of caffeine molecules within the NT14 SWNT cavity, focusing on both their structural and optoelectronic characteristics. Molecular mechanics and Density Functional Theory were utilized to model the dynamics of SWNTs and CA molecules, respectively. The interaction between these subsystems in CA-NT14 systems was modeled using a simple Lennard-Jones potential to account for van der Waals interactions. Our findings identified a stable diameter range of approximately 1.18 nm for energetically favorable configurations of CA@SWNTs. Our investigation revealed minimal impact on the bandgap of semiconducting SWNTs upon encapsulation of caffeine molecules, indicating that the hybrid structure maintains its ability to efficiently absorb visible light. Conversely, encapsulation within metallic SWNTs resulted in a noticeable reduction in the bandgap, limiting the absorption range due to altered optical properties arising from caffeine's interaction with the metallic SWNT's electronic structure. Furthermore, nonresonant Raman spectroscopy of semiconducting NT14, both before and after encapsulation, demonstrated evidence of charge transfer within CA@NT14 systems. Analysis of Raman modes indicated significant interactions between caffeine and NT14, influencing the electronic structure and optical properties of the hybrid material. DFT calculations provided insights into the elevated Fermi level in CA@NT14, confirming charge transfer from CA to NT14 and suggesting a type-II band alignment. Looking ahead, our future research

will focus on elucidating electronic transport characteristics, transmission spectra, I-V characteristics, and overall device yield of CA@NT14 hybrid systems using DFT calculations coupled with the Non-Equilibrium Green's Function (NEGF) formalism. These theoretical findings pave the way for experimental validation, which will further substantiate the efficacy and applicability of our computational predictions in practical applications, particularly in the development of advanced organic solar cells and other optoelectronic devices.

5 ACKNOWLEDGMENT

The work was supported by Moulay Ismail University Research Support (13-16) and French embassy in Morocco program. .

Author Contributions

All authors contributed to the study conception and design. Material preparation, data collection and analysis were performed by [Anass El Fatimy], [Mourad Boutahir], [Konstantinos Termentzidis], [Abdelhai Rahmani] and [Abdelali Rahmani]. The first draft of the manuscript was written by [Mourad Boutahir, Abdellah Elattar]. [Anass El Fatimy]. All authors reviewed the manuscript.

Conflicts of interest :

All authors declare no conflict of interest.

Data Availability Statement:

No Data associated in the manuscript

References

[1] Chiba, T., Hayashi, Y., Ebe, H., Hoshi, K., Sato, J., Sato, S., Pu, Y.-J., Ohisa, S., Kido, J.: Anion-exchange red perovskite quantum dots with ammonium iodine salts for highly efficient light-emitting devices. Nature Photonics **12**(11), 681–687 (2018)

[2] Kim, Y.S., Hong, S.H., Park, H.J., Kim, J.T., Jeong, H.J., Na, Y.S., Lim, K.R., Park, J.M., Kim, K.B.: Crystallization and phase transformation behavior of ticu-based bulk metallic glass composite with b2 particles. Journal of Alloys and Compounds **707**, 87–91 (2017)

[3] McMeekin, D.P., Wang, Z., Rehman, W., Pulvirenti, F., Patel, J.B., Noel, N.K., Johnston, M.B., Marder, S.R., Herz, L.M., Snaith, H.J.: Crystallization kinetics and morphology control of formamidinium–cesium mixed-cation lead mixed-halide perovskite via tunability of the colloidal precursor solution. Advanced Materials **29**(29), 1607039 (2017)

[4] Guerra, V.L., Altamura, D., Trifiletti, V., Colella, S., Listorti, A., Giannuzzi, R., Pellegrino, G., Condorelli, G.G., Giannini, C., Gigli, G., *et al.*: Implications of tio 2 surface functionalization on polycrystalline mixed halide perovskite films and photovoltaic devices. Journal of Materials Chemistry A **3**(41), 20811–20818 (2015)

[5] Green, M.A., Bremner, S.P.: Energy conversion approaches and materials for high-efficiency photovoltaics. Nature materials **16**(1), 23–34 (2017)

[6] Heeger, A.J.: 25th anniversary article: bulk heterojunction solar cells: understanding the mechanism of operation. Advanced Materials **26**(1), 10–28 (2014)

[7] You, J., Meng, L., Song, T.-B., Guo, T.-F., Yang, Y.M., Chang, W.-H., Hong, Z., Chen, H., Zhou, H., Chen, Q., *et al.*: Improved air stability of perovskite solar cells via solution-processed metal oxide transport layers. Nature nanotechnology **11**(1), 75–81 (2016)

[8] Hu, Z., Wang, J., Ma, X., Gao, J., Xu, C., Yang, K., Wang, Z., Zhang, J., Zhang, F.: A critical review on semitransparent organic solar cells. Nano Energy, 105376 (2020)

[9] Mellit, A., Benghanem, M.: A Practical Guide for Advanced Methods in Solar Photovoltaic Systems. Springer, ??? (2020)

[10] Wang, R., Xue, J., Meng, L., Lee, J.-W., Zhao, Z., Sun, P., Cai, L., Huang, T., Wang, Z., Wang, Z.-K., *et al.*: Caffeine improves the performance and thermal stability of perovskite solar cells. Joule **3**(6), 1464–1477 (2019)

[11] O'connell, M.J., Bachilo, S.M., Huffman, C.B., Moore, V.C., Strano, M.S., Haroz, E.H., Rialon, K.L., Boul, P.J., Noon, W.H., Kittrell, C., *et al.*: Band gap fluorescence from individual single-walled carbon nanotubes. Science **297**(5581), 593–596 (2002)

[12] Dürkop, T., Getty, S.A., Cobas, E., Fuhrer, M.: Extraordinary mobility in semiconducting carbon nanotubes. Nano letters **4**(1), 35–39 (2004)

[13] Landi, B.J., Raffaelle, R.P., Castro, S.L., Bailey, S.G.: Single-wall carbon nanotube–polymer solar cells. Progress in photovoltaics: research and applications **13**(2), 165–172 (2005)

[14] Polman, A., Knight, M., Garnett, E.C., Ehrler, B., Sinke, W.C.: Photovoltaic materials: Present efficiencies and future challenges. Science **352**(6283) (2016)

[15] Blackburn, J.L.: Semiconducting single-walled carbon nanotubes in solar energy harvesting. ACS Energy Letters **2**(7), 1598–1613 (2017)

[16] Wang, J., Peurifoy, S.R., Bender, M.T., Ng, F., Choi, K.-S., Nuckolls, C., Arnold, M.S.: Non-fullerene acceptors for harvesting excitons from semiconducting carbon nanotubes. The Journal of Physical Chemistry C **123**(35), 21395–21402 (2019)

[17] Jeon, I., Matsuo, Y., Maruyama, S.: Single-walled carbon nanotubes in solar cells. Single-Walled Carbon Nanotubes, 271–298 (2019)

[18] Cataldo, S., Salice, P., Menna, E., Pignataro, B.: Carbon nanotubes and organic solar cells. Energy & Environmental Science **5**(3), 5919–5940 (2012)

[19] Bachilo, S.M., Strano, M.S., Kittrell, C., Hauge, R.H., Smalley, R.E., Weisman, R.B.: Structure-assigned optical spectra of single-walled carbon nanotubes. science **298**(5602), 2361–2366 (2002)

[20] Kataura, H., Kumazawa, Y., Maniwa, Y., Umezu, I., Suzuki, S., Ohtsuka, Y., Achiba, Y.: Optical properties of single-wall carbon nanotubes. Synthetic metals **103**(1-3), 2555–2558 (1999)

[21] Boutahir, M., Chenouf, J., Mejía-López, J., Rahmani, A., Chadli, H., Rahmani, A.: Role of carbon nanotubes as an acceptor to enhance the photovoltaic performances of organic solar cells based on π-conjugated thiophene as a donor materials. International Journal of Energy Research **45**(11), 16242–16253 (2021)

[22] Boutahir, M., Fakrach, B., Mejía-López, J., Boutahir, O., Rahmani, A., Chadli, H., Rahmani, A., *et al.*: Short bandgap of porphyrin molecules (py) filled in a semiconducting single-walled carbon nanotube (py@ nt17) for highly efficient organic photovoltaic cells. Materials Science and Engineering: B **293**, 116456 (2023)

[23] El Fatemy, A., Boutahir, M., RAHMANI, A., Rahmani, A.: Van der waals interactions on the semiconducting single-walled carbone nanotube filled by porphyrin molecules: Structure optimisation and raman analysis. New Journal of Chemistry (2024)

[24] Fakrach, B., Fergani, F., Boutahir, M., Rahmani, A., Chadli, H., Hermet, P., Rahmani, A.: Structure and raman spectra of c 60 and c 70 fullerenes encased into single-walled boron nitride nanotubes: a theoretical study. Crystals **8**(3), 118 (2018)

[25] El Fatimy, A., Boutahir, M., Lopez J, M., El Khattabi, E., Rahmani, A.: Excitation energy transfer via electron transfer between a semi-conducting single walled-carbon nanotube and encapsulated zinc porphyrin or photovoltaic application. ChemistrySelect **9**(1), 202302799 (2024)

[26] El Fatimy, A., Boutahir, O., Rahmani, A., Boutahir, M., Mejía-López, J., Termentzidis, K., Rahmani, A.: Density functional theory calculations of optoelectronic properties of individual and encapsulated magnesium porphyrin in carbon nanotubes for organic nanohybrid solar cells. Energy Technology, 2301135 (2024)

[27] Holt, J.M., Ferguson, A.J., Kopidakis, N., Larsen, B.A., Bult, J., Rumbles, G., Blackburn, J.L.: Prolonging charge separation in p3ht- swnt composites using highly enriched semiconducting nanotubes. Nano letters **10**(11), 4627–4633 (2010)

[28] Chenouf, J., Boutahir, M., Fakrach, B., Rahmani, A., Chadli, H., Hermet, P., Mejía-López, J., Rahmani, A.: Encapsulation effect of π-conjugated quaterthiophene on the radial breathing and tangential modes of semiconducting and

metallic single-walled carbon nanotubes. Journal of Computational Chemistry **41**(28), 2420–2428 (2020)

[29] Dresselhaus, G., Riichiro, S., *et al.*: Physical Properties of Carbon Nanotubes. World scientific, ??? (1998)

[30] Boutahir, M., Abdelkader, S.A., Fakrach, B., Rahmani, A., Chadli, H., Rahmani, A.: Non resonant raman spectra of homogeneous and inhomogeneous individual dimers of single-walled carbon nanotubes (swnts). In: IOP Conference Series: Materials Science and Engineering, vol. 783, p. 012016 (2020). IOP Publishing

[31] Boutahir, M., Fakrach, B., Rahmani, A., Sbai, K., Chadli, H., Rahmani, A.: Wall thikness effects on the infrared spectra of multi-walled carbon nanotubes. In: IOP Conference Series: Materials Science and Engineering, vol. 783, p. 012017 (2020). IOP Publishing

[32] BOUTAHIR, M.: Functionalized graphene/polyaniline (pani@ grn) nanocomposites for organic solar cells. Available at SSRN 4270706

[33] Boutahir, O., Lakhlifi, S., Abdelkader, S.A.A., Boutahir, M., Rahmani, A., Chadli, H., Mejía-López, J., Rahmani, A.: Force-constant model for the vibrational modes in black-phosphorene and phosphorene nanoribbons (pnrs). Physica E: Low-dimensional Systems and Nanostructures **132**, 114757 (2021)

[34] Chenouf, J., Boutahir, M., Mejía-López, J., Rahmani, A., Fakrach, B., Chadli, H., Rahmani, A.: Predicting the structure configuration and raman analysis of caffeine molecules encapsulated into single-walled carbon nanotubes: Evidence for charge transfer. Solar Energy **232**, 204–211 (2022)

[35] Soler, J.M., Artacho, E., Gale, J.D., García, A., Junquera, J., Ordejón, P., Sánchez-Portal, D.: The siesta method for ab initio order-n materials simulation. Journal of Physics: Condensed Matter **14**(11), 2745 (2002)

[36] Dresselhaus, G., Dresselhaus, M.S., Saito, R.: Physical Properties of Carbon Nanotubes. World scientific, ??? (1998)

[37] Guha, S., Menendez, J., Page, J., Adams, G.: Empirical bond polarizability model for fullerenes. Physical Review B **53**(19), 13106 (1996)

[38] Boutahir, M., Rahmani, A., Chadli, H., Rahmani, A.: Electronic and vibrational properties of dimer of single-wall carbon nanotubes. In: Renewable and Sustainable Energy Conference (IRSEC), 2015 3rd International, pp. 1–5 (2015). IEEE

[39] Boutahir, M., Rahmani, A., Chadli, H., Rahmani, A.: Mechanical coupled vibrations in an individual double-walled carbon nanotube. The European Physical Journal Applied Physics **74**(2), 24605 (2016)

[40] Jamal, C., Mourad, B., Brahim, F., Abdelhai, R., Hassane, C., Abdelali, R.: Vibrational study of bithiophene encapsulated in single wall carbon nanotube using the infrared calculations. In: 2020 1st International Conference on Innovative Research in Applied Science, Engineering and Technology (IRASET), pp. 1–6 (2020). IEEE

[41] Rahmani, A., Benoit, M., Benoit, C.: Signature of small rings in the raman spectra of normal and compressed amorphous silica: A combined classical and ab initio study. Physical Review B **68**(18), 184202 (2003)

[42] Rahmani, A., Sauvajol, J.-L., Rols, S., Benoit, C.: Nonresonant raman spectrum in infinite and finite single-wall carbon nanotubes. Physical Review B **66**(12), 125404 (2002)

[43] Umari, P., Pasquarello, A., Dal Corso, A.: Raman scattering intensities in α-quartz: A first-principles investigation. Physical Review B **63**(9), 094305 (2001)

[44] Pandey, L., Risko, C., Norton, J.E., Bredas, J.-L.: Donor–acceptor copolymers of relevance for organic photovoltaics: a theoretical investigation of the impact of chemical structure modifications on the electronic and optical properties. Macromolecules **45**(16), 6405–6414 (2012)

[45] Kalbac, M., Kavan, L., Dunsch, L., Dresselhaus, M.: Development of the tangential mode in the raman spectra of swcnt bundles during electrochemical charging. Nano letters **8**(4), 1257–1264 (2008)